Ain Shams Engineering Journal 13 (2022) 101719

Contents lists available at ScienceDirect

Ain Shams Engineering Journal

journal homepage: www.sciencedirect.com

Speed control and torque ripple minimization of SRM using local unimodal sampling and spotted hyena algorithms based cascaded PID controller

Hossam Kotb [a,*], Ahmed H. Yakout [b], Mahmoud A. Attia [b], Rania A. Turky [c], Kareem M. AboRas [a]

[a] Department of Electrical Power and Machines, Faculty of Engineering, Alexandria University, Alexandria, Egypt
[b] Department of Electrical Power and Machines, Faculty of Engineering, Ain Shams University, Cairo, Egypt
[c] Department of Electrical Engineering, Faculty of Engineering and Technology, Future University in Egypt, Cairo, Egypt

ARTICLE INFO

Article history:
Received 26 November 2021
Revised 31 December 2021
Accepted 18 January 2022
Available online 28 January 2022

Keywords:
Switched reluctance motor
Cascaded PID
Speed control
Torque ripple minimization

ABSTRACT

This paper proposes the use of two recent optimization techniques, called the Local Unimodal Sampling (LUS) and the Spotted Hyena Optimizer (SHO), to optimally tune cascaded PID controller designed while controlling the speed and reducing the torque ripples of the switched reluctance motor. The proposed implementation of these algorithms has the advantage of better convergence and lower computational efforts when compared to other optimization techniques. To demonstrate the effectiveness of the proposed cascaded PID controller using LUS and SHO, they are compared to other controller designs present in previous literature, specifically the cascaded fractional-order PID (FOPID) controller. Results show that the PID controller is more superior to the FOPID controller and that the SHO-based cascaded PID controller leads to less current and torque ripples with better speed response. The study is implemented at different loading conditions. The results are presented in the form of a time-domain simulation conducted via MATLAB/SIMULINK.

1. Introduction

In the last decade, the switched reluctance motor (SRM) has been extensively studied by researchers due to its low cost, simple construction, wide range of speed, high starting torque, and flexible control with fault tolerance [1,2]. The SRM performance has been greatly improved due to advances in power converters and control techniques [3]. Nowadays, with the rapid development of the industry, SRM is widely applied in textile machines, electric vehicles, robotic control applications, and aviation industries [4–6]. However, due to the switched power supply and doubly salient nature, the SRM often suffers from some drawbacks such as nonlinear magnetic characteristics, undesirable torque ripples, and acoustic noise [7–9] which in turn affect the reliability and safety of the system greatly. Moreover, since it is difficult to achieve accurate control by only using traditional regulation, researchers have been working on improving the SRM performance by means of new methods of control and design [10-15].

Some complex control techniques were proposed in the literature to reduce torque ripples in SRM drives, such as torque sharing function (TSF), direct torque control (DTC), feedback control, and average torque control (ATC) methods [16–19]. In [16], both DTC and TSF control strategies were implemented to suppress the torque ripples of 12/8 pole SRM. The authors also discussed the responses to changes in speed and load torque. While in [17], a predictive DTC technique was proposed to enhance the motor speed and torque response. It showed the effectiveness of the predictive control compared to conventional DTC methods. Another control approach proposed in [18] was able to maintain the desired average torque at the desired speed by using the ATC algorithm. This technique was improved in [19] by using multi-objective optimized control parameters. Furthermore, a sliding mode control technique was introduced in [20] to compensate for low-frequency oscillations in the torque output of the SRM. In [21], an optimal commutation strategy for SRM was presented to

* Corresponding author.
E-mail address: hossam.kotb@alexu.edu.eg (H. Kotb).

Peer review under responsibility of Ain Shams University.

Production and hosting by Elsevier

https://doi.org/10.1016/j.asej.2022.101719

Nomenclature

ACO	Ant colony optimization
ATC	Average torque control
$\overrightarrow{b_l}$, $\overrightarrow{b_u}$	Lower and upper boundaries of the search space
$\overrightarrow{B}$, $\overrightarrow{E}$	Coefficient vectors
$\overrightarrow{d}$	Initial search range
$\overrightarrow{D_h}$	Distance between the spotted hyena and prey
DTC	Direct torque control
FF	Fitness function
FOPID	Fractional order proportional-integral-derivative
GA	Genetic algorithm
$\overrightarrow{H}$	Exploitation vector
i	Phase current
K_{d1}, K_{d2}	Derivative gains of cascaded controller
K_{i1}, K_{i2}	Integral gains of cascaded controller
K_{p1}, K_{p2}	Proportional gains of cascaded controller
L	Phase inductance
LUS	Local Unimodal Sampling
N	Number of spotted hyenas
$\overrightarrow{P}$	Position vector of the spotted hyena
$\overrightarrow{P_h}$	Position of the first best spotted hyena
$\overrightarrow{P_k}$	Position of the other spotted hyenas
$\overrightarrow{P_p}$	Position vector of the prey
PID	Proportional-integral-derivative
PSO	Particle swarm optimization
q	Reduction factor
$\overrightarrow{R_1}$, $\overrightarrow{R_2}$	Random vectors
SHO	Spotted hyena optimizer
SRM	Switched reluctance motor
t_{sim}	Simulation time
T_{phase}	Torque per phase
TSF	Torque sharing function
x	Current iteration
θ	Rotor position
λ	Integral order
μ	Derivative order

increase the torque production capacity of the motor and greatly reduce torque ripple. Moreover, a detailed literature survey about classical SRM torque ripples minimization techniques was presented in [4].

On the other hand, other researchers preferred to use a simpler controller design approach where numerous optimization techniques based PID controllers have been proposed for optimal speed and torque response [22–25]. For example, Ant Colony Optimization (ACO) and Genetic Algorithm (GA) techniques were introduced in [22] and [23] for tuning the PID gains for 8/6 SRM drive. By this algorithm, the SRM speed regulation was improved in terms of tracking fast setpoint and regulatory changes. Another optimal tuning of the PID controller for speed control of the SRM was proposed in [24] using Particle Swarm Optimization (PSO). The work concentrated on the design of feedback PID parameters to achieve the minimum integral quadratic error of speed. Furthermore, an adaptive Fuzzy control was applied in [25] to regulate the speed of SRM but the torque performance was relatively poor. In [26], Ant Lion-based cascaded Fractional Order PID controller (FOPID) was designed to enhance the speed and torque profile of a 6/4 SRM drive. While Authors of [27] found the optimal design of the SRM parameters which lead to better torque and speed performance. Authors of [28] found that changing core materials by using soft Magnetic Composite will enhance the SRM performance.

Furthermore, various control techniques have been introduced over the years for current regulation of SRM [29]. Current chopping control was the most popular method for current control of SRM because of its model independence and quick dynamic response [30]. Another intelligent controller based on iterative learning control was presented in [31,32] as an alternative to the hysteresis controller. In addition, some researchers have introduced a linear model of SRM to overcome the problem of nonlinearity in SRM [33,34]. Complex control strategies were presented in the literature such as model predictive control [35,36], dead-beat control [37,38], adaptive control [39], and sliding mode control [40,41]. The main drawbacks of the aforementioned techniques are complexity, high current ripples, slow response, and sensitivity to model uncertainties. Therefore, the main contributions of this paper are:

- Designing an efficient cascaded PID controller for improving the speed response of the 6/4 poles SRM drive while minimizing the torque ripples.
- Using two recent optimization techniques to design the optimal gains of the cascaded PID controller, which are the Local Unimodal Sampling (LUS) and the Spotted hyena optimizer (SHO).
- Evaluating the effectiveness of the proposed cascaded PID controller design under different load conditions.
- Comparing the results of the proposed controller by the FOPID controller presented in the previous literature.

Moreover, the paper consists of five sections: Section 1 is an introductory section, while Section 2 introduces the discussed case study. This is followed by the problem formulation and a summary of the proposed optimization techniques in Section 3. Both results and discussions are presented in Sections 4 and 5, respectively. And finally, Section 6 concludes the paper.

2. Case study

The case study model is shown in Fig. 1 which consists of 6/4, three-phase SRM of rated power 60 kW [26]. The SRM is fed by a 3-phase converter with a 240 V dc source. To control the switching frequency of phase currents, a position sensor is connected to the rotor with turn-on and turn-off angles of 45° and 75°, respectively. The SRM model is simulated using MATLAB/Simulink with the following parameters: stator pole arc = 30°, rotor pole arc = 32°, stack length = 51 mm, stator diameter = 82.1 mm, rotor diameter = 40 mm, number of windings per pole = 72 turns, stator resistance = 0.05 Ω, inertia = 0.05 kg.m^2 and friction = 0.02 N.m.s. Moreover, speed control and torque ripple elimination are achieved by adding a cascaded PID controller. The first PID controller is connected in the outer loop to control the speed with a reference speed of 2000 rpm and whose output is limited to 250 (the SRM rated current). While the second PID controller is connected in the inner loop for current control thus reducing the torque ripples. The SRM performance can be described by the following torque equation [23]:

$$T_{phase}(\theta, i) = \frac{1}{2} i^2 \frac{dL(\theta, i)}{d\theta} \quad (1)$$

where the torque per phase T_{phase} depends on the variation of inductance L with rotor position θ and phase current i, while the total torque produced by the three phase currents can be expressed by the following equation [23]:

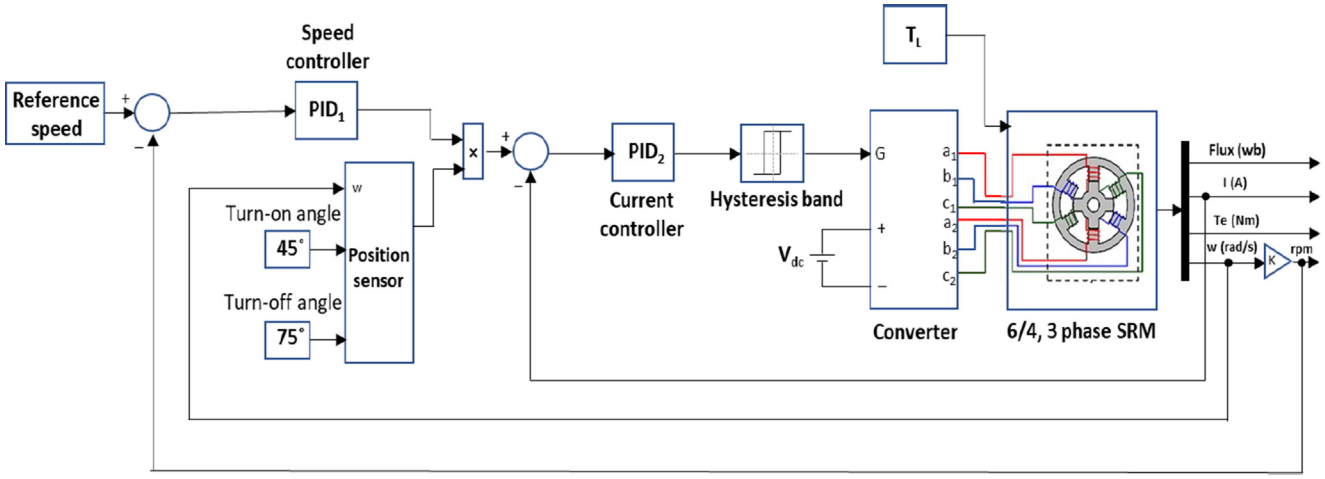

Fig. 1. Block diagram of the SRM model equipped with a cascaded PID controller.

$$T_{total}(\theta, i) = \sum_{phases} \frac{1}{2} i^2 \frac{dL(\theta, i)}{d\theta} \quad (2)$$

The variation of the three phase flux (or inductance), three phase currents, and the magnetization curve for our case study are shown in Fig. 2(a-c). The proposed objective function and optimization algorithms will be presented in the next section.

3. Problem formulation

Here, the parameters of the two PID controllers (outer speed controller and inner current controller) will be optimized using LUS and SHO optimization techniques to improve the speed response and minimize ripples in speed, current, and torque of the SRM presented in Section 2. To obtain such improvement, the

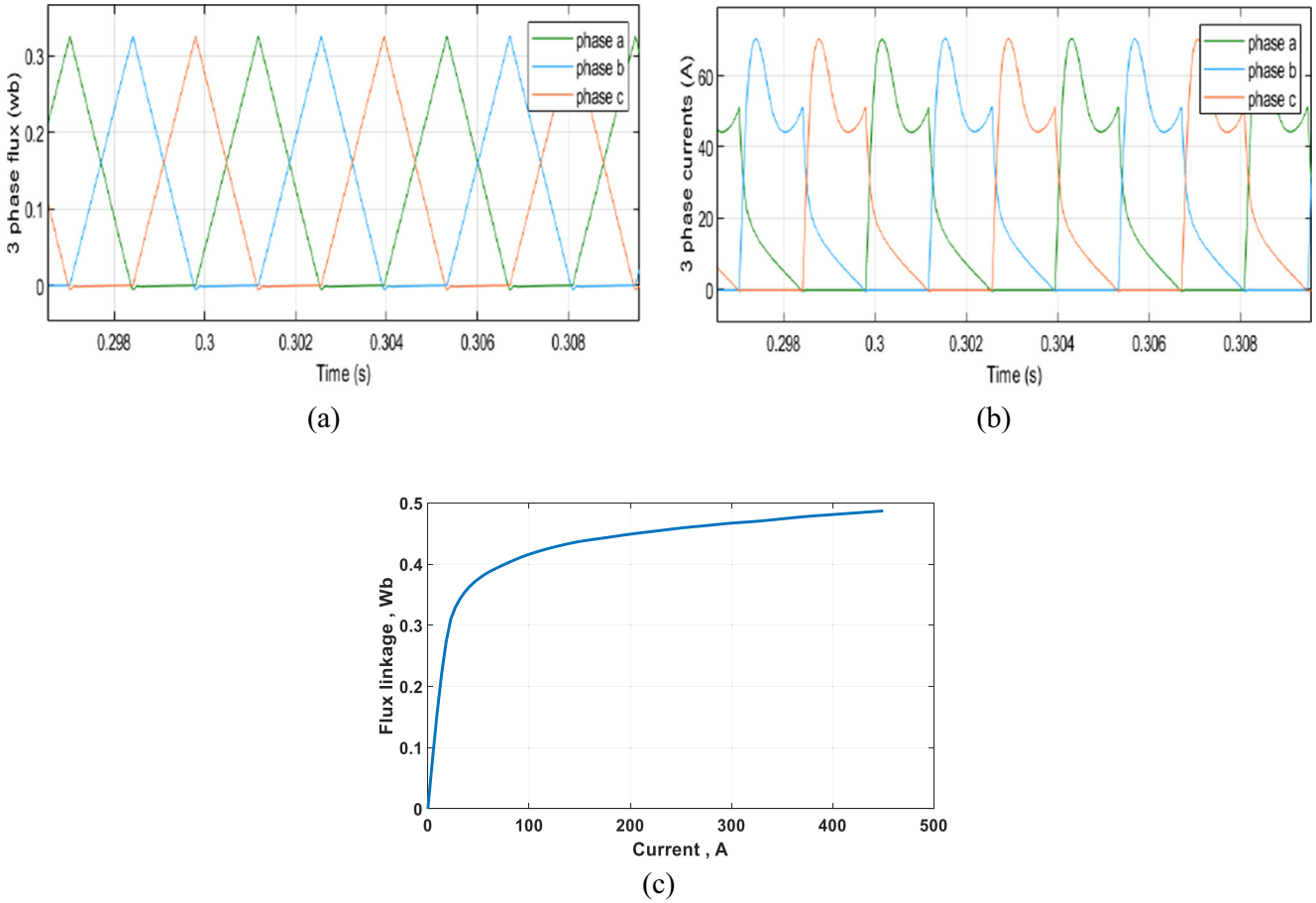

Fig. 2. Variation of (a) 3 phase flux (or inductance), (b) 3 phase currents, and (d) magnetization curve.

proposed fitness function (FF) is the integral sum of squared error of the speed and current using equation (3) as follows [22]:

$$\text{Minimize} FF = \int_0^{t_{sim}} (speed\ \ error)^2 + (current\ \ error)^2 dt \tag{3}$$

where t_{sim} is the simulation time in s. Furthermore, the objective function is subject to the following constraints:

$$\begin{cases} K_{p1,min} \le K_{p1} \le K_{p1,max} \\ K_{i1,min} \le K_{i1} \le K_{i1,max} \\ K_{d1,min} \le K_{d1} \le K_{d1,max} \\ K_{p2,min} \le K_{p2} \le K_{p2,max} \\ K_{i2,min} \le K_{i2} \le K_{i2,max} \\ K_{d2,min} \le K_{d2} \le K_{d2,max} \end{cases} \tag{4}$$

where K_{p1}, K_{i1}, and K_{d1} are the proportional, integral, and derivative gains, respectively of the PID speed controller. K_{p2}, K_{i2}, and K_{d2} are the proportional, integral, and derivative gains, respectively of the PID current controller. Moreover, a simple stability analysis based on the Ziegler-Nichols method is applied in which the proportional gains of speed and current controllers are increased in steps from 20 to 100. Results show that the system remains stable due to the presence of a limiter on the output of the speed controller. However, the current ripples increase as the proportional gain increases. Based on this, the studied controller's gains range is taken to be between 0 and 20 for stability reasons. Moreover, the optimal gains of the two PID controllers will be obtained using the Local unimodal sampling algorithm and the Spotted hyena optimizer algorithm that will be presented in the next subsections.

3.1. Local unimodal sampling (LUS)

The LUS optimization technique uses local sampling to reduce the sample range during optimization by moving a single agent throughout the search space. LUS method is one of the optimization techniques that does not suffer from trapping in local optimum solutions [42]. This is due to its variable sampling range which makes it superior over several fixed range optimization algorithms as Hill Climber and Simulated particle Annealing algorithms [43]. The main steps of the LUS algorithm can be summarized as follows:

1. Initialize the current position $\vec{x}$ in the search space to a random value.
2. Set the initial search range $\vec{d}$ to cover the entire search space as follows [42]:

$$\vec{d} \leftarrow \vec{b_u} - \vec{b_l} \tag{5}$$

where $\vec{b_u}$ and $\vec{b_l}$ are the upper and lower boundaries of the search space, respectively.

Repeat the following steps until the stopping criterion is checked (fitness is reached with a certain tolerance of 0.000001 or maximum number of iterations is100).

- Select a random vector $\vec{a} \sim U(-\vec{d}, \vec{d})$.
- Create the new potential position $\vec{y}$ as follows [42]:

$$\vec{y} = \vec{x} + \vec{a} \tag{6}$$

- If the fitness at position $\vec{y}$ is less than the fitness at position $\vec{x}$, then update the position $\vec{x} \leftarrow \vec{y}$. Otherwise, decrease the search range as follows [42]:

$$\vec{d_{new}} = q \times \vec{d} \tag{7}$$

where q is a reduction factor used to decrease the new sampling range. The flowchart of the LUS algorithm is shown in Fig. 3. For more details, check [42].

3.2. Spotted hyena optimizer (SHO)

SHO is a relatively new optimization technique. It is based on the spotted hyena's behavior of hunting. The advantage of the SHO algorithm is that its search agents are updated by a factor that combines all the optimal solutions from the previous iteration. The mathematical model of the SHO algorithm can be represented by the following equations [44]:

$$\vec{D_h} = |\vec{B} . \vec{P_p}(x) - \vec{P}(x)| \tag{8}$$

$$\vec{P}(x+1) = \vec{P_p}(x) - \vec{E} . \vec{D_h} \tag{9}$$

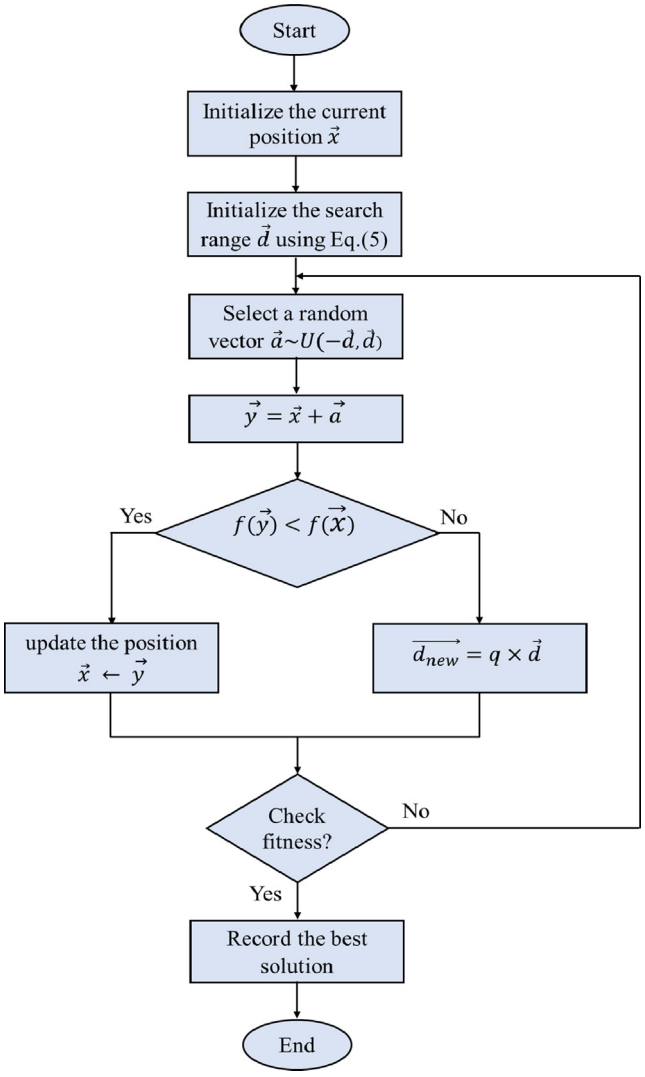

Fig. 3. LUS algorithm flowchart.

where $\overrightarrow{D_h}$ represents the distance between the spotted hyena and prey,x is the current iteration, $\vec{B}$ and $\vec{E}$ are coefficient vectors, $\vec{P}$ denotes the position vector of spotted hyena, and $\overrightarrow{P_p}$ represents the position vector of prey. The vectors $\vec{B}$ and $\vec{E}$ can be estimated as follows [44]:

$$\vec{B} = 2.\overrightarrow{R_1} \tag{10}$$

$$\vec{E} = 2\vec{H}.\overrightarrow{R_2} - \vec{H} \tag{11}$$

where $\overrightarrow{R_1}$ and $\overrightarrow{R_2}$ are random vectors from [0,1]. The exploitation vector $\vec{H}$ can be calculated as follows [44]:

$$\vec{H} = 5 - (Iteration \times (\frac{5}{Max_{iteration}}) \tag{12}$$

$$\overrightarrow{D_h} = |\vec{B}.\overrightarrow{P_h} - \overrightarrow{P_k}| \tag{13}$$

$$\overrightarrow{P_k} = \overrightarrow{P_h} - \vec{E}.\overrightarrow{D_h} \tag{14}$$

$$\overrightarrow{C_h} = \overrightarrow{P_k} + \overrightarrow{P_{k+1}} + \cdots + \overrightarrow{P_{k+N}} \tag{15}$$

where $\overrightarrow{P_h}$ represents the position of the first best spotted hyena and $\overrightarrow{P_k}$ indicates the position of other spotted hyenas. The number of spotted hyenas N can be estimated as follows:

$$N = count_i(\overrightarrow{P_h}, \overrightarrow{P_{h+1}}, \overrightarrow{P_{h+2}}, \cdots, (\overrightarrow{P_h} + \vec{M})) \tag{16}$$

where i is the number of solutions and $\vec{M}$ is a random vector from [0.5, 1]. The best solution can be updated as follows:

$$\vec{P}(x+1) = \frac{\overrightarrow{C_h}}{N} \tag{17}$$

where $\overrightarrow{C_h}$ represents a group of N optimal solutions. Then, the search agent positions are updated with new fitness calculations, and all these steps are repeated until the best position is achieved (reaching a certain tolerance or a maximum number of iterations of 100). The steps of the SHO algorithm can be summarized as shown in Fig. 4. More details are given in [44]. The simulation results and discussions will be presented in Sections 4 and 5.

4. Simulation results and comparisons

Three loading conditions are studied and simulated: Case 1: No load, Case 2: Static load for a torque of 100 N.m, and Case 3: Dynamic load is simulated for a 10 s interval, where a torque of 100 N.m. is applied at t = 3 s and then removed at t = 8 s. The LUS and SHO-based PID gains for both speed and current controllers at the three previous loading conditions are presented in Table 1. Moreover, the SRM time response with PID coefficients optimized using LUS and SHO algorithms is validated by comparing the results obtained to the results of three cascaded FOPID controllers designed in previous literature which are optimized by GA [23], PSO [24], and Ant-Lion [26]. Moreover, the optimal FOPID gains, the integral, and the derivative orders (λ, μ) are presented in Table 2 using different optimization techniques. Furthermore, Table 3 shows the optimal fitness function using different controllers for the three studied cases. It can be observed that the SHO-PID controller has the least fitness function compared to other controllers.

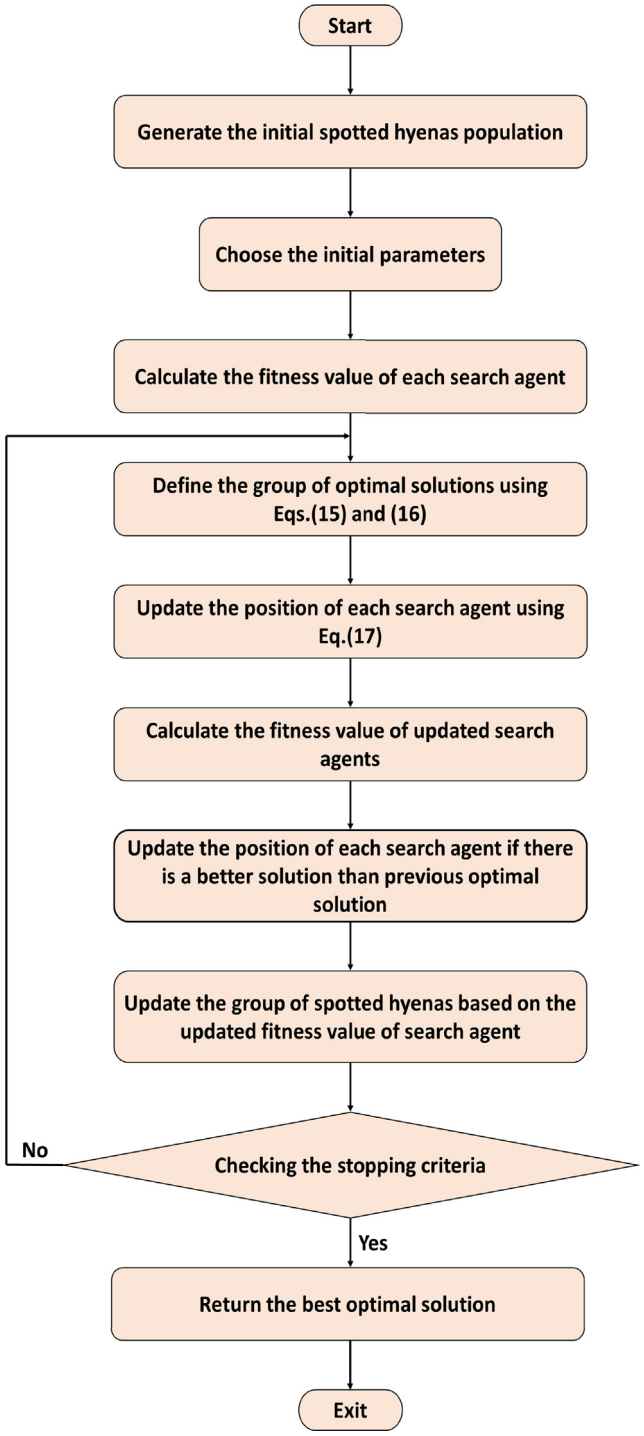

Fig. 4. SHO algorithm flowchart.

4.1. Case 1: no-load torque (t = 0)

The simulation results for this case are shown in Fig. 4. By applying a reference speed of 2000 rpm, the SHO algorithm provides the best speed response compared to other techniques. As illustrated in Fig. 5(a), the SHO and LUS techniques provide the best transient and steady-state due to the lowest settling time (fast response) and lowest steady-state error. The LUS algorithm has slightly better speed performance than Ant-Lion and PSO techniques. Unfortunately, the GA technique provides the low speed performance due to high settling time. Fig. 5(b) shows the phase

Table 1
Gains of PID controllers based on LUS and SHO algorithms for different cases.

Algorithm	Speed controller			Current controller		
	K_{p1}	K_{i1}	K_{d1}	K_{p2}	K_{i2}	K_{d2}
LUS	4.9209	8.9603	0.1244	9.7779	3.6249	8.9451
SHO	12.2799	10.8923	0	18.6819	20	18.7407

Table 2
Gains and orders of FOPID controllers based on different optimization algorithms.

Algorithm	Speed controller					Current controller				
	K_{p1}	K_{i1}	K_{d1}	λ	μ	K_{p2}	K_{i2}	K_{d2}	λ	μ
GA [23]	3.85	7.25	8.382	0.78	0.27	4.26	6.58	5.27	0.64	0.42
PSO [24]	5.38	5.79	4.89	0.4	0.24	5.24	4.39	6.17	0.28	0.71
Ant-Lion [26]	4.75	5.85	2.39	0.31	0.52	3.24	5.25	1.98	0.54	0.83

Table 3
Optimal fitness function using different controllers.

Controller	CASE 1 No-load torque	CASE 2 T = 100 N.m.	CASE 3 Dynamic load torque
GA-FOPID [23]	0.0199	0.4528	0.7443
PSO-FOPID [24]	0.0081	0.4334	0.1997
Ant-Lion-FOPID [26]	0.0081	0.4352	0.7249
LUS-PID (proposed)	0.0099	0.0165	0.0201
SHO-PID (proposed)	0.0075	0.0161	0.0183

current ripples of the no-load case. It can be observed that the lowest current ripples can be achieved based on the SHO and LUS algorithms. However, the Ant-Lion and PSO algorithms show higher current ripples, and the GA exhibits the highest ripples of current. Fig. 5(c) shows that all optimization techniques have the same torque ripples behavior for the no-load condition.

4.2. Case 2: Static load torque (t = 100n.m)

The simulation results for this case are shown in Fig. 6. Similar to the no-load case, the speed response of the SRM is greatly improved using the SHO algorithm as shown in Fig. 6(a). The SHO-based PID controller provides a very fast speed response with fewer speed ripples and zero steady-state error. However, the PSO and Ant-lion algorithms show slightly less settling time than the LUS algorithm, but they have higher speed ripples and steady-state error than the LUS. The GA provides the lowest speed response in terms of high settling time, high-speed ripples, and high steady-state error of the speed which accounts for 8.5%. Fig. 6(b) shows the current ripples of phase current during the static load torque. Both SHO and LUS algorithms provide the lowest current ripples which cannot exceed 100 A. But the Ant-lion, GA, and PSO algorithms exhibit high current ripples of no more than 200A. In addition, the reduction of torque ripples during load can be achieved through the SHO and LUS algorithms as shown in Fig. 6(c). The other optimization algorithms exhibit very high torque ripples unacceptable for the SRM performance.

4.3. Case 3: Dynamic load torque

In this case, a load torque of 100 N.m. is applied to the SRM drive at t = 3 s, then removed at t = 8 s. The time-domain simulation of the dynamic disturbance is shown in Fig. 7. Similar to the previous cases, the SHO algorithm provides the best speed response as shown in Fig. 7(a). It can be observed that the speed is not affected by the disturbance torque at t = 3 and 8 s which is a great feature of the SHO algorithm. Although the LUS algorithm provides a fast-speed response and is not affected by disturbance, it exhibits some allowable overshoot. Also, the PSO and Ant-lion algorithms exhibit a slightly lower speed response with some steady-state error. It can be seen that the GA exhibits the lowest speed response and is highly affected by the disturbance torque at 3 s and 8 s.

Fig. 7(b) shows the phase current profile under the disturbance load from 0 to 10 s. The lowest current ripples can be achieved with the SHO algorithm while the GA algorithm shows the highest current ripples. More details about the current ripples before and during the disturbance torque are shown in Fig. 7(c) and 6(d) respectively. The lowest current ripples can be achieved by the SHO algorithm while the GA shows the highest current ripples. All algorithms give the same minimized torque ripples at intervals from 0 to 3 s and from 8 to 10 s as shown in Fig. 7(e) and (f). Moreover, the control action (output) signals of both speed and current controllers are shown in Figs. 8 and 9, respectively using different controllers. It can be seen that by using SHO algorithm, the speed controller produces low ripples that act as the required reference current, while the current controller produces suitable required high frequency pulses after passing through the hysteresis band to achieve the low current ripples mentioned above.

4.4. Comparison between PID and FOPID controllers using LUS and SHO algorithms

This section aims to compare the performance of the proposed PID controllers with the FOPID controllers using LUS and SHO algorithms. The convergence curve of the fitness function using LUS and SHO algorithms is shown in Fig. 10 for 50 iterations. It can be seen that the SHO is faster than LUS and has better convergence. Moreover, the optimal gains of the LUS and SHO based FOPID controllers are given in Table 4. Results show that the SHO-PID controllers provide lower current ripples compared to other controllers as shown in Fig. 11. However, the speed response and torque ripples are almost the same for all cases.

5. Discussions

5.1. Case 1: no-load torque (t = 0)

In Fig. 5(a), the speed response settling time is about 2.5, 1, 1, 0.7, and 0.1 s using GA-FOPID, PSO-FOPID, Ant-FOPID, LUS-PID, and SHO-PID, respectively. Therefore, the SHO-PID has the fastest speed response. In Fig. 5(b), the current ripple accounts for 29, 11, 11, 6, and 4 A using GA-FOPID, PSO-FOPID, Ant-FOPID, LUS-PID, and SHO-PID, respectively. Therefore, the SHO-PID produces

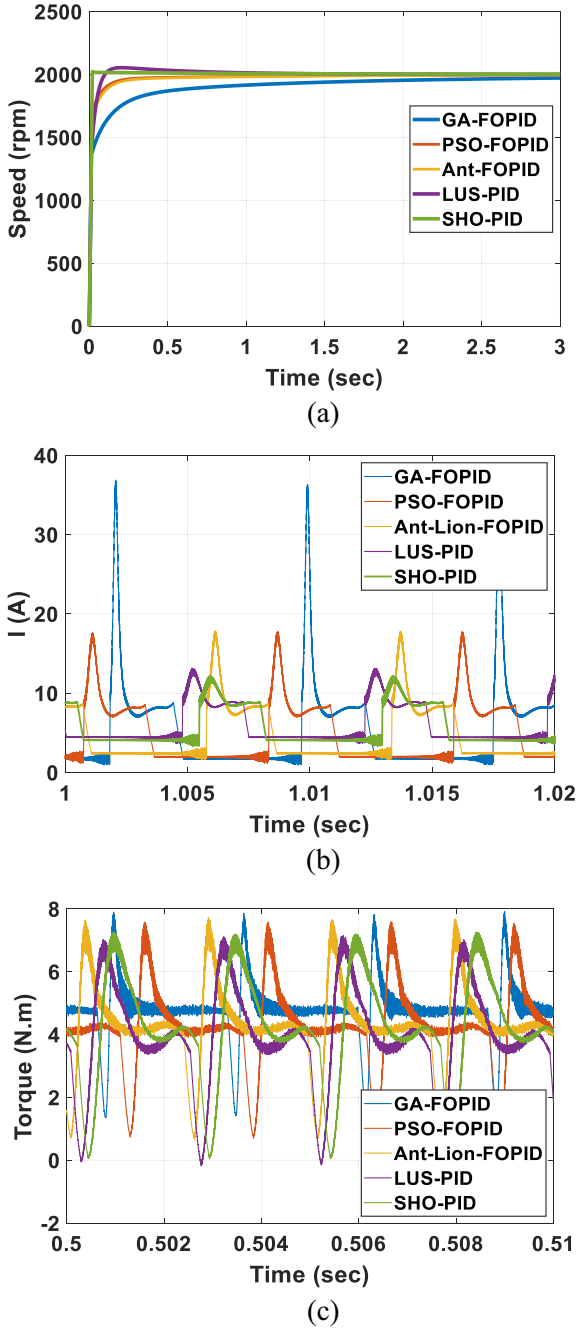

Fig. 5. Time response of (a) speed, (b) phase current and (c) total torque for different controller structure and optimization algorithms at no-load.

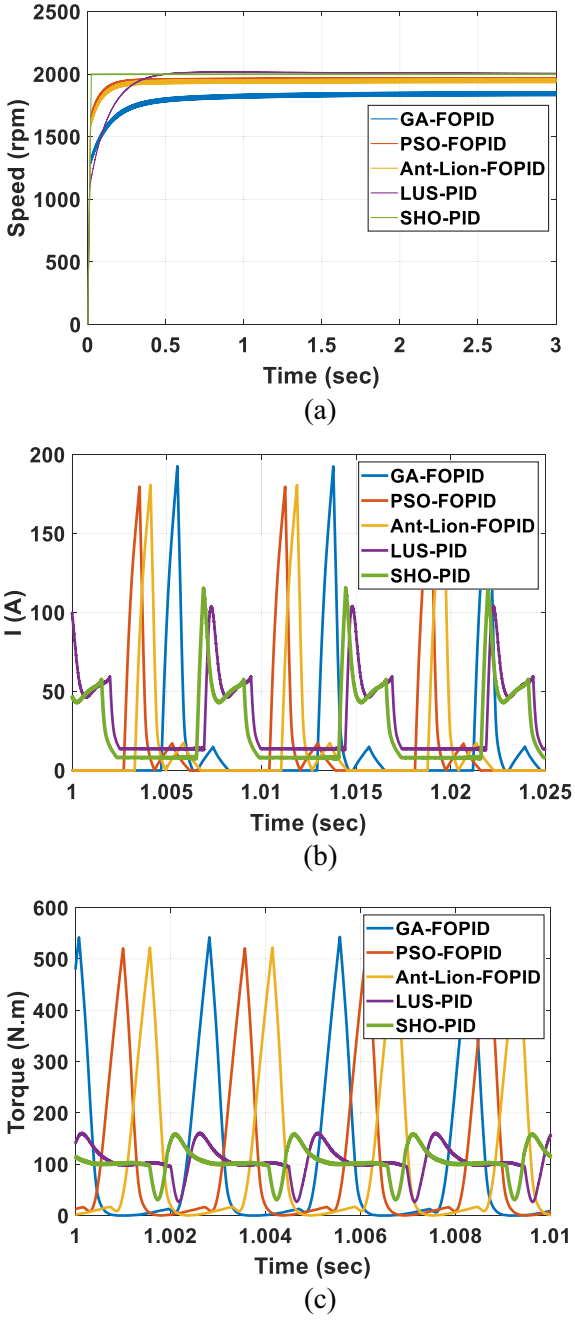

Fig. 6. Time response of (a) speed, (b) phase current and (c) total torque based on different controller structures and optimization algorithms with static load (T = 100).

the lowest current ripple. In Fig. 5(c), the torque ripple is approximately the same using all techniques which accounts for 8 Nm.

5.2. Case 2: Static load torque (t = 100 nm)

In Fig. 6(a), the speed response settling time is about 3.5, 2, 2, 1.5, and 0.1 s using GA-FOPID, PSO-FOPID, Ant-FOPID, LUS-PID, and SHO-PID, respectively. Therefore, the SHO-PID has the fastest speed response. In Fig. 6(b), the current ripple accounts for 190, 175, 175, 50, and 55 A using GA-FOPID, PSO-FOPID, Ant-FOPID, LUS-PID, and SHO-PID, respectively. Therefore, the suggested controllers produce the lowest current ripple. In Fig. 6(c), the torque ripple accounts for 520, 510, 510, 100, and 100 Nm using GA-FOPID, PSO-FOPID, Ant-FOPID, LUS-PID, and SHO-PID, respectively. Therefore, the suggested controllers produce the lowest torque ripple.

5.3. Case 3: Dynamic load torque

In Fig. 7(a), at the no load interval, Although the SHO and LUS based PID controllers have a smaller settling time compared to the fractional controllers, the LUS exhibits some allowable overshoot. Once 100 Nm torque is applied, the speed response of FOPID controllers shows some steady-state error. While Fig. 7(b-f) show

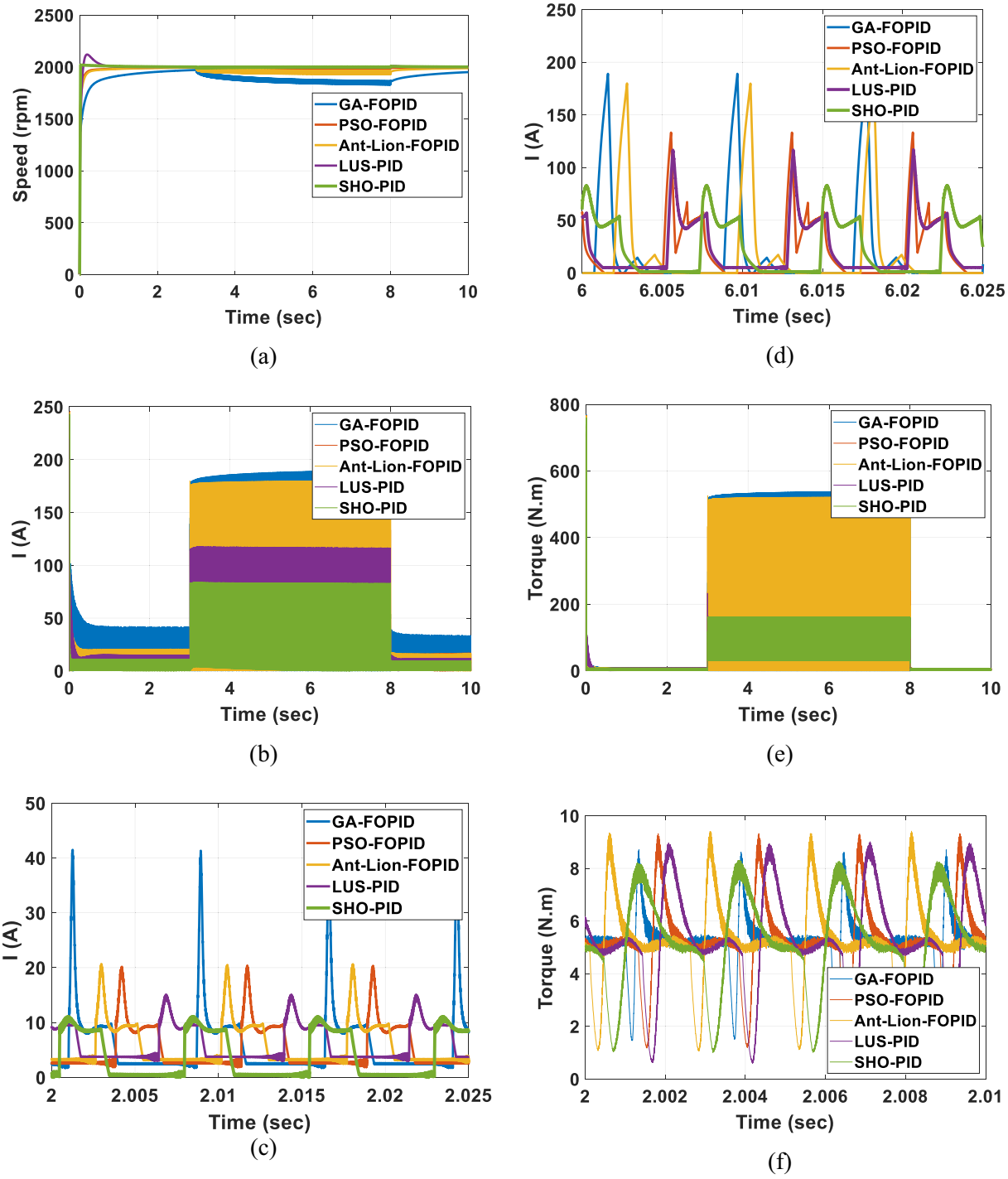

Fig. 7. Time response of (a) speed, (b) phase current profile, (c) zoomed phase current when T = 0, (d) zoomed phase current when T = 100 N.m, (c) torque profile, and (f) zoomed torque at no load.

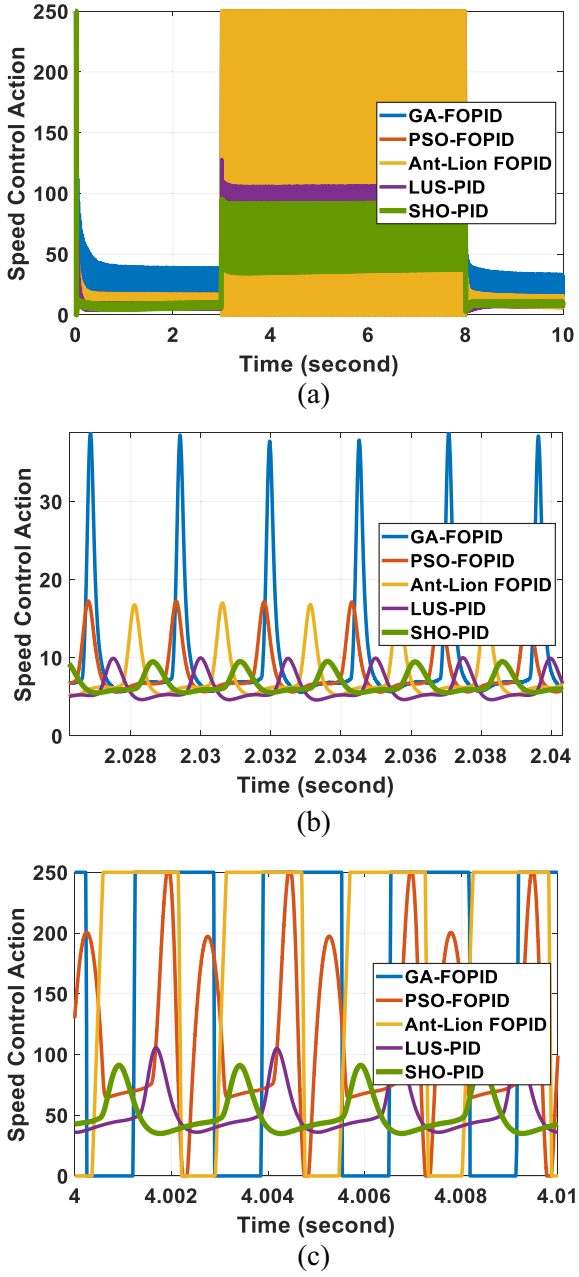

Fig. 8. Speed control action signal for (a) dynamic load, (b) no load torque, and (c) static load torque of 100 N.m.

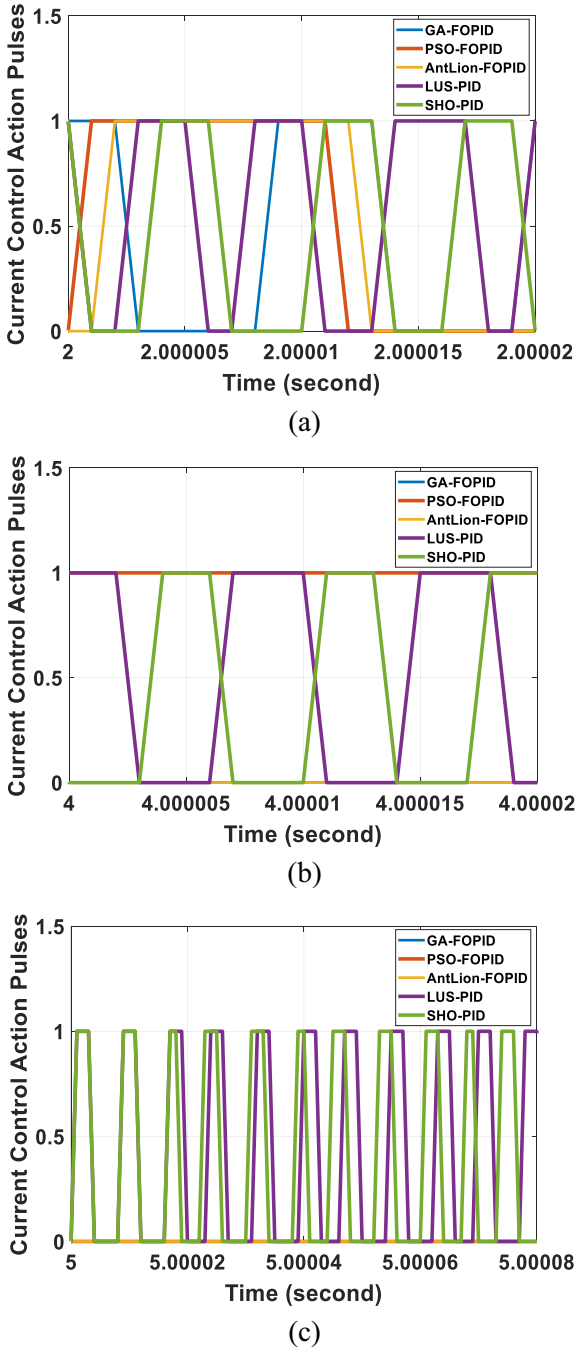

Fig. 9. Current control action signal for (a) no load torque, (b) static load torque of 100 N.m zoomed after 4 s, and (c) static load torque of 100 N.m zoomed after 5 s.

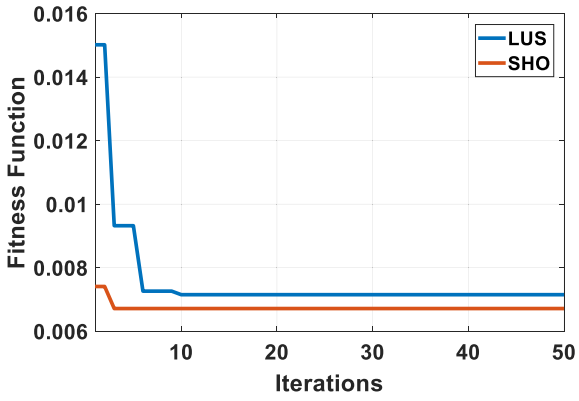

Fig. 10. Convergence curve of LUS and SHO algorithms.

that the current and torque ripples are almost the same as in case 1 and case 2.

6. Conclusions

In this paper, a cascaded PID controller using Local unimodal sampling algorithm and Spotted hyena optimizer is proposed to control the speed of a switched reluctance motor as well as reduce the torque ripples. The Spotted hyena optimizer technique leads to a PI-PID structure while the Local unimodal sampling algorithm leads to a full PID-PID structure. Moreover, comparisons with existing optimization techniques based on cascaded Fractional-order PID controllers such as Ant-Lion, Particle swarm optimization, and Genetic Algorithm show that a cascaded PID controller leads to better speed, current, and torque responses with no speed steady-state error and less current and torque ripples whether the load was static or dynamic. But when it comes to comparing the two proposed cascaded PID controllers, the SHO-PID controller has successfully proven the best speed response with the lowest torque ripples in all cases because the merit of the Spotted hyena optimizer algorithm in updating its search agents by a factor that combines all optimal solutions from the previous iteration. While the Local unimodal sampling algorithm comes in second place with slightly lower performance than the Spotted hyena optimizer algorithm. Moreover, the fractional-order PID controller using Ant-Lion and Particle swarm optimization produces higher current and torque ripples and slower speed response than SHO and LUS based PID. Finally, GA-FOPID produces the highest current and torque ripples with the lowest speed performance. For future studies, the improved switched reluctance motor can be applied to electric vehicles, pumps, and other industrial applications.

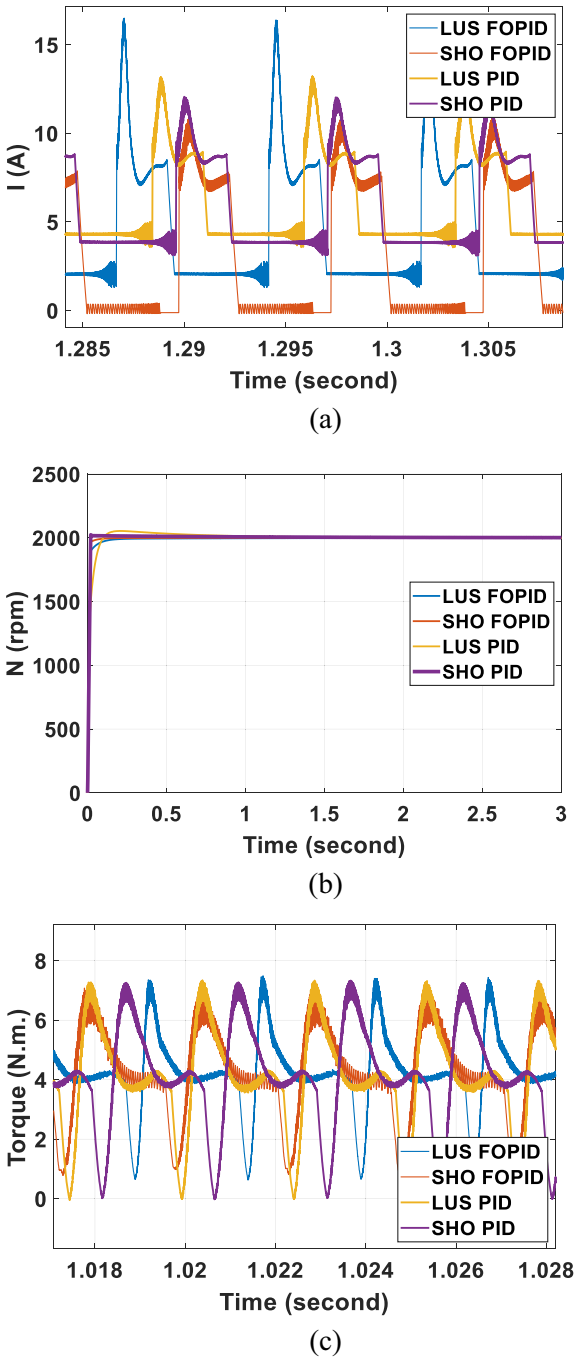

Fig. 11. Time response of (a) phase current, (b) speed and (c) total torque using different controllers at no-load.

Table 4
Optimal gains of FOPID controllers using LUS and SHO algorithms.

Algorithm		K_p	K_i	K_d	λ	μ
LUS-FOPID	Speed controller	4.69	7.83	16.42	0.13	0.11
	Current controller	3.33	13.11	14.63	0.45	0.61
SHO-FOPID	Speed controller	8.68	2.68	0	0.1	0.9
	Current controller	5.56	5.54	15.68	0.1	0.1

Declaration of Competing Interest

The authors declare that they have no known competing financial interests or personal relationships that could have appeared to influence the work reported in this paper.

References

[1] Ye J, Bilgin B, Emadi A. An offline torque sharing function for torque ripple reduction in switched reluctance motor drives. IEEE Trans Energy Convers 2015;30(2):726–35.
[2] Cai Y, Wang C, Ju C, Tianjin HX. Research on torque model based on pretreatment method for switched reluctance motor. 2018 13th IEEE Conference on Industrial Electronics and Applications (ICIEA). IEEE; 2018.
[3] Saha N, Panda AK, Panda S. Speed control with torque ripple reduction of switched reluctance motor by many optimizing liaison technique. J Electr Syst Inf Technol 2018;5(3):829–42.
[4] Gan C, Wu J, Sun Q, Kong W, Li H, Hu Y. A review on machine topologies and control techniques for low-noise switched reluctance motors in electric vehicle applications. IEEE Access 2018;6:31430–43.
[5] Lukman GF, Nguyen XS, Ahn J-W. Design of a low torque ripple three-phase SRM for automotive shift-by-wire actuator. Energies 2020;13(9):2329. doi: https://doi.org/10.3390/en13092329.
[6] Bogusz P. A switched reluctance motor control method limiting the maximum dc source current in the low-speed range. Bull Pol Acad Sci Tech Sci 2016;64:197–206.
[7] Liang J, Jiang JW, Callegaro AD, Bilgin B, Dong J, Reeves D, et al. Prediction of acoustic noise and vibration of a 24/16 traction switched reluctance machine. IET Electr Syst Transp 2020;10(1):35–43.
[8] Qin Y, He C, Shao X, Du H, Xiang C, Dong M. Vibration mitigation for in-wheel switched reluctance motor driven electric vehicle with dynamic vibration absorbing structures. J Sound Vib 2018;419:249–67.
[9] Rezig A, Boudendouna W, Djerdir A, N'Diaye A. Investigation of optimal control for vibration and noise reduction in-wheel switched reluctance motor used in electric vehicle. Math Comput Simul 2020;167:267–80.
[10] Elamin M, Yasa Y, Sozer Y, Kutz J, Tylenda J, Wright RL. Effects of windows in stator and rotor poles of switched reluctance motors in reducing noise and vibration. 2017 IEEE International Electric Machines and Drives Conference (IEMDC). IEEE; 2017.
[11] Guyadec ML, Gerbaud L, Vinot E, Reinbold V, Dumont C. Use of reluctance network modelling and software component to study the influence of electrical machine pole number on hybrid electric vehicle global optimization. Math Comput Simul 2019;158:79–90.
[12] Omaç Z, Cevahir C. Control of switched reluctance generator in wind power system application for variable speeds. Ain Shams Eng J 2021;12(3):2665–72. doi: https://doi.org/10.1016/j.asej.2021.01.009.
[13] Mbadiwe EI, Bin Sulaiman E. Design and optimization of outer-rotor permanent magnet flux switching motor using transverse segmental rotor shape for automotive applications. Ain Shams Eng J 2021;12(1):507–16.
[14] Labiod C, Srairi K, Mahdad B, Benchouia MT, Benbouzid MEH. Speed control of 8/6 switched reluctance motor with torque ripple reduction taking into account magnetic saturation effects. Energy Procedia 2015;74:112–21.
[15] Xu A, He K, Cao Y. Torque ripple reduction of SRM using optimized voltage vector in DTC. 2016 IEEE Vehicle Power and Propulsion Conference (VPPC). IEEE; 2016.
[16] Maksoud HA. Torque ripple minimization of a switched reluctance motor using a torque sharing function based on the overlap control technique. Eng Technol Appl Sci Res 2020;10(2):5371–6.
[17] Abdelfadil R, Számel L. Predictive direct torque control of Switched Reluctance Motor for Electric Vehicles drives. Period Polytech Electr Eng Comput Sci 2020. doi: https://doi.org/10.3311/ppee.15496.
[18] Jamil MU, Kongprawechnon W, Chayopitak N. Average Torque Control of a Switched Reluctance Motor Drive for Light Electric Vehicle Applications. IFAC-PapersOnLine 2017;50:11535–40.
[19] Hamouda M, Abdel Menaem A, Rezk H, Ibrahim MN, Számel L. Numerical estimation of switched reluctance motor excitation parameters based on a simplified structure average torque control strategy for electric vehicles. Mathematics 2020;8(8):1213. doi: https://doi.org/10.3390/math8081213.
[20] Gao X, Wang X, Li Z, Zhou Y. A review of torque ripple control strategies of switched reluctance motor. Int J Contr Autom 2015;8(4):103–16.
[21] Ren P, Zhu J, Jing Z, Guo Z, Xu A. Minimization of torque ripple in switched reluctance motor based on MPC and TSF. IEEJ Trans Electr Electron Eng 2021;16:1535–43.
[22] Ibrahim HE-SA, Ahmed MSS, Awad KM. Speed control of switched reluctance motor using genetic algorithm and ant colony based on optimizing PID controller. In: ITM Web Conf, vol. 16, 2018, p. 01001.
[23] Saha N, Panda S. Speed control with torque ripple reduction of switched reluctance motor by Hybrid Many Optimizing Liaison Gravitational Search technique. Eng Sci Technol Int J 2017;20(3):909–21.
[24] Nimisha KK, Senthilkumar R. Optimal tuning of PID controller for switched reluctance motor speed control using particle swarm optimization. 2018 International Conference on Control, Power, Communication and Computing Technologies (ICCPCCT). IEEE; 2018.
[25] Zhang C, Ming Z, Su Z, Cai Z. An advanced robust method for speed control of switched reluctance motor. Rev Sci Instrum 2018;89.
[26] Prasad ES, Ram BVS. Ant-lion optimizer algorithm based FOPID controller for speed control and torque ripple minimization of SRM drive system. 2016 International Conference on Signal Processing, Communication, Power and Embedded System (SCOPES). IEEE; 2016.
[27] Mamede ACF, Camacho JR, Araujo RE, Guimaraes GC. Effects analysis of design parameters on three-phase 6/4 and four-phase 8/6 switched reluctance machines performance. 2020 International Conference on Electrical Machines (ICEM). IEEE; 2020.
[28] Vijayakumar K, Joseph Basanth A, Karthikeyan R, Sivakumar V, Balamurugan N, Shanmuga Sundaram C. Influence of iron powder core on the switched reluctance motor performance enhancement. Mater Today 2020;33:2255–63.
[29] Fang G, Pinarello Scalcon F, Xiao D, Vieira R, Grundling H, Emadi A. Advanced control of switched reluctance motors (SRMs): A review on current regulation, torque control and vibration suppression. IEEE Open J Ind Electron Soc 2021;2:280–301.
[30] Peng F, Ye J, Emadi A. A digital PWM current controller for switched reluctance motor drives. IEEE Trans Power Electron 2015. 1–1.
[31] El-Kharahi E, El-Dessouki M, Lindh P, Pyrhönen J. Toward including the effect of manufacturing processes in the pre-estimated losses of the switched reluctance motor. Ain Shams Eng J 2015;6(1):121–31.
[32] Lai C, Zheng Y, Labak A, Kar NC. Investigation and analysis of iterative learning-based current control algorithm for switched reluctance motor applications. 2014 International Conference on Electrical Machines (ICEM). IEEE; 2014.
[33] Ahmad SS, Narayanan G. Linearized modeling of switched reluctance motor for closed-loop current control. IEEE Trans Ind Appl 2016;52(4):3146–58.
[34] Huang H-N, Hu K-W, Wu Y-W, Jong T-L, Liaw C-M. A current control scheme with back EMF cancellation and tracking error adapted commutation shift for switched-reluctance motor drive. IEEE Trans Ind Electron 2016;63 (12):7381–92.
[35] Li X, Shamsi P. Inductance surface learning for model predictive current control of switched reluctance motors. IEEE Trans Transp Electrif 2015;1 (3):287–97.
[36] Li X, Shamsi P. Model predictive current control of switched reluctance motors with inductance auto-calibration. IEEE Trans Ind Electron 2016;63 (6):3934–41.
[37] Zhang X, Yang Q, Ma M, Lin Z, Yang S. A switched reluctance motor torque ripple reduction strategy with deadbeat current control and active thermal management. IEEE Trans Veh Technol 2020;69(1):317–27.
[38] Ahmad SS, Narayanan G. Predictive control based constant current injection scheme for characterization of switched reluctance machine. IEEE Trans Ind Appl 2018;54(4):3383–92.
[39] Ganji B, Heidarian M, Faiz J. Modeling and analysis of switched reluctance generator using finite element method. Ain Shams Eng J 2015;6(1):85–93.
[40] Manolas I, Papafotiou G, Manias SN. Sliding mode PWM for effective current control in Switched Reluctance Machine drives. 2014 International Power Electronics Conference (IPEC-Hiroshima 2014 - ECCE ASIA). IEEE; 2014.
[41] Hu K, Ye J, Velni JM. Sliding mode current control of mutually coupled switched reluctance machines using a three-phase voltage source converter. 2019 IEEE Energy Conversion Congress and Exposition (ECCE). IEEE; 2019.
[42] Mohanty PK, Sahu BK, Panda S. Tuning and assessment of proportional–integral–derivative controller for an automatic voltage regulator system employing local unimodal sampling algorithm. Electr Power Compon Syst 2014;42(9):959–69.
[43] Micev M, Calasan M, Ali ZM, Hasanien HM, Abdel Aleem SHE. Optimal design of automatic voltage regulation controller using hybrid simulated annealing – Manta ray foraging optimization algorithm. Ain Shams Eng J 2021;12 (1):641–57.
[44] Dhiman G, Kumar V. Spotted hyena optimizer: A novel bio-inspired based metaheuristic technique for engineering applications. Adv Eng Softw 2017;114:48–70.

Hossam Kotb received the B.Sc., M.Sc., and Ph. D. degrees in Electrical Engineering from the Faculty of Engineering, Alexandria University, Alexandria, Egypt, in 2009, 2013, and 2020, respectively. His Ph.D. research work is focused on the performance enhancement of renewable energy conversion systems. He is currently an Assistant Professor with the Department of Electrical Power and Machines, Faculty of Engineering, Alexandria University. He is a reviewer for many international journals. His research interests include power system control, optimization, electrical drives, modern control techniques, smart grids, and renewable energy systems.

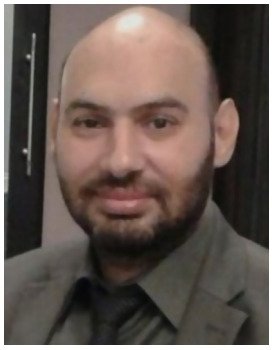

Ahmed H. Yakout is currently an Associate Professor at Faculty of Engineering, Ain Shams University, Cairo, Egypt. He received his PhD in electrical engineering from Strathclyde university, Glasgow, UK, 2010. Earlier, he received his B.Sc., M.Sc. degrees from the electrical power and machines department, Faculty of Engineering, Ain Shams university in 2000, 2005 respectively. His main research interests include modern control techniques, renewable energy and electrical power systems analysis, stability and control.

Mahmoud A. Attia, He is currently working as an Associate Professor of electrical power engineering at Ain Shams University**.** He received B. Sc., M.Sc. and Ph.D. in electrical engineering from Ain Shams University (ASU), Egypt in 2005, 2010 and 2015 respectively. He has joined ASU teaching stuff since 2007. He authored many journal and conference papers. He is a reviewer for power component and systems journal, Ain Shams Engineering Journal Elsevier and International Transactions on Electrical Energy Systems. 2009, He was in Technical committee of ASU international conference ASCEE-3. He was a Member of "Continuous Improvement & Quality Assurance Unit of Faculty of engineering ASU" till 2017. He is the author of books 'Optimal Allocation of FACTS Devices in Electrical Power Systems: A Genetic Algorithm Based Approach', in April 2013 and 'Enhancing Power System Performance with Growing Wind Power Penetration: optimal Allocation of FACTS', in July 2015 LAP LAMBERT Academic Publishing. He contributed in book 'Sustainable Energy Technologies and Systems', LAP LAMBERT Academic Publishing, 2019. He is an editorial member of i-manager's Journal on Circuits and Systems. He is an editor in chief of i-manager's Journal on Instrumentation and Control Engineering. His research areas include the applications of artificial intelligence, evolutionary and heuristic optimization techniques to power system operation, planning, and control.

Rania A. Turky received his B.Sc. and M.Sc. degrees in Electrical Power Engineering from Ain Shams University, Faculty of Engineering, Cairo, Egypt, in 2004 and 2010, respectively. She is now pursuing PhD degree. Her research interests include modern control techniques, power systems dynamics and control, energy storage systems, renewable energy systems, and smart grid.

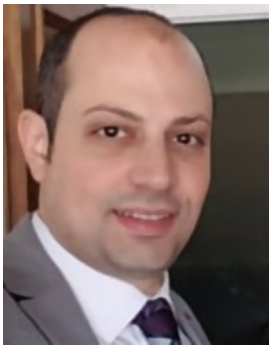

Kareem M. AboRas received his B.Sc., M.Sc. and Ph.D. degrees in Electrical Engineering from Alexandria University, Faculty of Engineering, Alexandria, Egypt, in 2010, 2015, and 2020, respectively. His Ph.D. research work is focused on the performance enhancement of renewable energy conversion systems. Currently, he is an Assistant Professor at the Electrical Power and Machines Department, Faculty of Engineering, Alexandria University. Mr. AboRas is a reviewer in IET journal. His research interests include power electronics, control, drives, power system and renewable energy systems.